International Journal on Interactive Design and Manufacturing (IJIDeM) (2019) 13:967–980
https://doi.org/10.1007/s12008-019-00547-w

ORIGINAL PAPER

Prediction of a flying droplet landing over a non-flat substrates for ink-jet applications

Ivan Arango[1] · Leonardo Bonil[1] · David Posada[1] · Javier Arcila[2]

Received: 30 November 2018 / Accepted: 15 January 2019 / Published online: 18 February 2019

Abstract
Printing with inkjet technology has found new forms of application in the industry and in this article we study this technology focused on printing on non-flat surfaces. Since there is no print history over distances greater than 1 mm due to the rupture phenomenon, an initial quality standard is defined to measure achievements in a relative manner. An interactive method is used that requires the user to approach the machine in multiple analyzes of different types. The first approach is a mathematical model this model was constructed to predict the drop distance of the drop in the non-planar substrate with respect to the planned one in the flat substrate, taking into account that most of the drops fall to different heights presenting a greater or lesser state of development the phenomena present in the flight. The results allow to initiate a process of compensation that avoids the distortion of the figure to improve the printing resolution. The results are validated using a relative quality through industrial ink-jet printer with heads capable of injecting functional fluids. The initial result indicates that in standard surface printing with print relative quality already defined, it can be used only for low resolution formats with thick lines, and the result can be improved when the original figure is treated by compensating the distance between the numerical prediction and the initial objective.

Keywords Ink-jet printing · Droplet trajectory · Non-flat substrates · Compensation · Functional fluid

1 Introduction

Ink-jet printing has emerged as a promissory technology in fields such as a manufacturer of sensing devices [1, 2], the printing of living cells [3, 4], tissues [5], ceramic dental teeth [6], UV inks on cylindrical surfaces [7], and surface coatings [8], among other fields [9]. Ink-jet technology is classified in two categories according to the type of the print head: Continuous ink-jet (CIJ) [10] and drop-on-demand (DoD).

The advantage of ink-jet printing is the ability to operate in a drop on demand mode. This improves the flexibility of the process and contributes to a substantial saving in the costs of the inks [11]. Drop on demand ink-jet technology have a higher compatibility with various functional materials and their ability to reliably deposit them onto a substrate [12]. The main challenges of ink-jet printing include high resolution printing and precision in new application fields.

Drop-on-demand print heads are predominant in the industry [13]. Tiny droplets (6–150 pL) are expelled through the nozzles of the print head, wich has a piezoelectric actuator and, when given an applied voltage the resulting deformation ejects the droplets onto the substrate [14].

The inks implemented in ink-jet technology are generally composed by a solvent and pigments particles, and are usually used for decorative purposes. The use of the ink-jet as additive manufacturing technology (AM) [15, 16] has allowed the development of functional fluids (FF), which are a mixture of solvent and solid particles made of silver, polymers, gold, living cells, etc. The difference between inks and functional fluids is not well established in the literature

✉ Ivan Arango
iarango@eafit.edu.co

Leonardo Bonil
lbonilla@eafit.edu.co

David Posada
dposada4@eafit.edu.co

Javier Arcila
jarcila@corona.com.co

[1] EAFIT University, Medellín, Colombia

[2] Corona Group, Medellin, Colombia

and, in the majority of the cases the term "ink" for AM purposes is still used.

Ink-jet applications tend to print 2D patterns onto flat substrates, but several times, non-flat substrates are presented in fields such as tissues [17], electrical devices [18] and polymer substrates [19]. Other application recently introduced in the market is the printing over cylindrical containers [7]. The print heads have rows of nozzles on a flat distribution, which makes it difficult to print patterns onto a non-flat substrate since the print head nozzles are not equidistant from the substrate and this tends to distort the original pattern. To achieve good quality printing onto non-flat substrates, the droplets must be positioned onto the substrate with great precision, taking the substrate curvature into account. As a consequence, the study of ink-jet technology with non-flat substrates is important in the progress and versatility of this technology.

Another issue with ink-jet printing onto flat and non-flat substrates is the trajectory of the flying drop, which, when given a print head velocity, takes a parabolic trajectory. This trajectory must be taken into account in order to predict the position of the drop onto the substrate, and consequently, correct the error produced by this movement. Jin et al [20] studied the compensation of the movement of the print head path taking the trajectory of the ink-jet droplets. This study is centered on flat substrates and had not taken neither the droplet aerodynamics into account, nor the spreading factor at the moment of drop impact onto the substrate and the influence of the FF properties on the aerodynamics and stability of the drops.

The presence of particles in the functional fluids affect properties such as surface tension, viscosity and density [21]. The system in the printer are also special when works with nano and micro fluids [22]. Several authors have carried out studies about these properties such as Krieger and Dougherty [23] and Poletto and Joseph [24]. A group of dimensionless numbers can be used to quantify some characteristics of the FF such as printability, stability and flow behaviour. The most common dimensionless numbers used in ink-jet technology are: Weber (We), Reynolds (Re), Ohnesorge (Oh) and Bond (Bo). Some numbers can be expressed as a function of other dimensionless numbers such as the Capillary number ($Ca = We/Re$), and printability ($Z = Re/We^{1/2}$).

The aerodynamics of the droplet in ink-jet technology is still a field to study [25]. Some studies have been carried out about the type of flow in the gap between the print head and the substrate, and its influence over the droplets [26, 27]. Link et al. [28] had concluded that there is a significant shift in the trajectory of the droplets when the velocity of the substrate is about 8–10 m/s. The stability of the flying droplet must be taken into account. The energy drag must be less than the surface energy of the droplet in order to avoid the pinch-off of the flying droplets. Some authors, such as Pilch, Erdman [29] and Theofanous [30], had researched this phenomenom.

Functional fluids are not considered monofluids, because they are composed of different solutions that directly affect their properties, such as surfactants, pigments, functional elements, binders, humectants, etc. For this reason, its physical and rheological properties are unique.

The machines that work in conjunction with a computer, which are made up of mechanical hardware and software, that work on complex physical systems; they require multiple software tools for their design, manufacture and operation. Therefore, a methodology to work with these is the interactive design that allows to maximize the use of different applications in which the user receives information that evaluates, modifies and reintroduces in the following. An example of this method is the investigation of Barone [31].

The present paper aims to analyze the final position of a single droplet onto the substrate using mathematical models, taking into account the print head velocity, aerodynamics, spreading factor and functional fluids properties. The prediction of the position of the droplet onto non-flat substrates is presented together with an algorithm to correct the relative distance between droplets in order not to deform the image.

2 Methodology

In this research an interactive approach method is used because there are multiple tools, knowledge and methods that should be used to achieve the end, and in the development of this approach is made to the machine in which partial results are obtained that the user evaluates, modifies, validates and reintroduces in the machine.

In the development of the mathematical model, mathematical editors are used, who first individually describe partial phenomena such as: parabolic flight, aerodynamic resistance, fluid mechanics, step by step, a mathematical definition is being built integrating these areas, which by means of the use of simulators describes the difference between the drop of a real drop and a theoretical drop, with this information a compensation system can be made that must be introduced in the file that processes the RIP of the machine, achieving the compensation of the drop of all the drops.

The mathematical model is presented in the next section, which is based on an energy balance. With a deductive method, an algorithm is developed to predict where a drop will impact the non-flat substrate, and then compensate the distance between the head print and the substrate. This algorithm is validated in an inkjet printing machine with industrial print heads. After analyzing the results, an inductive method is applied to optimize the solution.

The experiments to validate the mathematical model are presented in Fig. 1. Experiments *a* and *b*, in which the movement of the print head is parallel to the *x*-axis shows the effect of the trajectory of the flying drops, due to the fact that the distance between the print head and the substrate is the same for each line, producing parallel lines. Experiments *c* and *d*, in which the movement of the print head is parallel to the *y*-axis, emphasizes the effect of the distance between the substrate and print head, this characteristic produces curved lines.

The equipment test includes: Projecta® Evo/plotter dg1400-700, print head Xaar® 1001 GS12 of 12–84 picoliter per drop with 7 gray scale sizes and 360 nozzles per inch. The machine was adjusted in binary mode, which implies a train of drops of 7 × 12 pL. The solid size is a length of 90–100 mm and has a height of 30–40 mm. The printing process was performed in two orientations, separated by 90° separated. The figure to be printed had parallel lines separated by 5 mm.

The characteristics of the printing fluids selected were: viscosity of 12–20 cP and surface tension of 3250 m N m^{-1}. Density of 1200 kg/m^3 at 40 °C. The functional fluids used for conventional printers are composed of water, oil, functional elements and UV protection properties. The functional fluids selected were, black (Endeka®) at 1300 kg/m^3, red TEP13301 at 1270 kg/m^3 and brown TEB16617 at 1350 kg/m^3 (Colorobbia®) These functional fluids will be used for functional printing on tiles that will be cooked at 1000 °C. Bond graph paper at 80 g/m^2 was used as a substrate. Tests were conducted in a place with an altitude of 1530 m, 0.84 atmospheres and the functional fluid temperature of 40–42 °C.

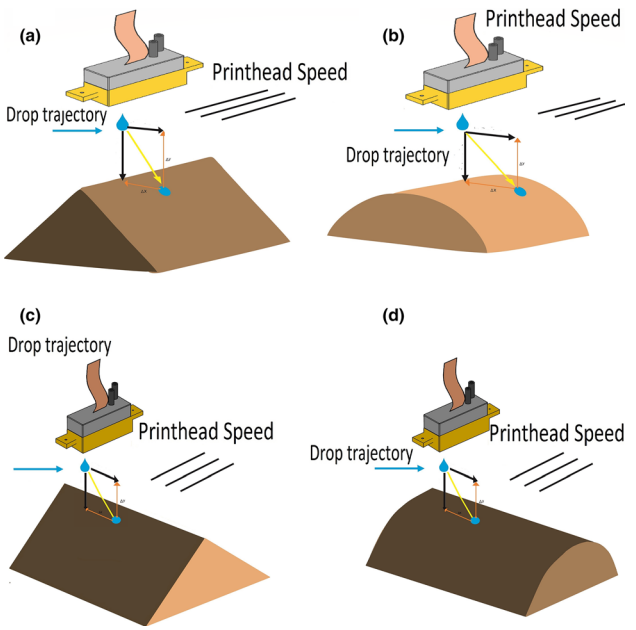

Fig. 1 Relative movement between the printhead and the substrate, **a** perpendicular to the spine of the triangular prism with movement on the "x" axis, **b** perpendicular to the spine of the truncated cylinder with movement on the "x" axis, **c** perpendicular to the spine of the triangular prism with movement in the "y" axis, **d** perpendicular to the spine of the truncated cylinder with movement in the "y" axis

A different quality from the standard for industrial inkjet printing is defined. The best relative impression is that obtained in an inkjet printer (300 dpi non grayscale) making lines at a distance head-substrate of 2 mm, the quality of relative impression is established in qualitative terms expressed as a percentage for any distance greater than the standard quality. The level of quality indices are referring to the dispersion and distortion of the drops outside the line. In [12], satellite drops are the drops that are formed when the main drop undergoes the drop breakup effect.

2.1 Mathematical model

The FF properties affect several factors of the droplets such as: drop formation, traveling distance and spread on the substrate. Some dimensionless numbers are common in ink-jet industry, and are used to establish some characteristics of the FF. Reynolds number shows the relation between inertial forces and viscous forces, and as consequence, it is useful to control the drop breakup. The Reynolds number is given by Eq. (1).

$$Re = \frac{\rho D V}{\eta} \tag{1}$$

where ρ is the density of the fluid, D is the diameter of the drop, V is the velocity of the drop (or fluid) assuming media velocity zero, and η is the dynamic viscosity. The main parameter to establish droplet breakup is the Weber Number (We). This dimensionless number shows the relation between inertial forces and capillary forces. This number is used to establish the stability of a flying droplet and is represented in Eq. (2). The Ohnesorge number (Oh) is a combination of the We and Re numbers (See Eq. 3). The interval at which the Ohnesorge number should be when analyzed in the inkjet printing process, is $1 < \mathrm{Oh} > 0.1$. In values greater than 1, the viscosity does not allow the fluid separation and drop formation. At values below 0.1 the generation of satellite drops is high. The symbol σ in Eqs. (2) and (3) is the surface tension.

$$We = \frac{\rho D V^2}{\sigma} \tag{2}$$

$$Oh = \frac{\eta}{\sqrt{\sigma \rho D}} \tag{3}$$

Once the droplet leaves the print head, there is a combination of energies on the droplet. The total energy with which the droplet leaves the print head (E_0) is shown in Eq. (4).

$$E_0 = E_{k0} + E_{s0} + E_{p0} \tag{4}$$

where E_{k0} is the kinetic energy, initially E_{s0} is the surface tension energy and E_{p0} is the potential energy. According to Wu et al. [32], the drop is not completely spherical, having an increase in the deformation when it is close to the substrate. But initially purposes of speed calculation, the shape is assumed to be spherical. Potential energy is often negligible, but, since the surface of the substrate has a variation in its distance, the path of the drop will also vary. Therefore the potential energy must be taken into account. Rewriting Eq. (4), the total initial energy is:

$$E_0 = \frac{1}{2}\rho_f \frac{4}{3}\pi\left(\frac{D_0}{2}\right)^2 V_0^2 + 4\pi\left(\frac{D_0}{2}\right)^2 \sigma + mgZ_0 \tag{5}$$

where ρ_f is the density of the fluid, D_0 is the diameter of the droplet, V_0 is the initial velocity of the drop, m is the mass and Z_0 is the distance between the nozzle plate and the substrate. As the drop travels, its velocity decreases, due to non-conservative forces such as the drag force. Considering a state of energy just before the impact of the droplet onto the substrate, Eq. (6) shows the balance of energy between the two states. The potential energy when the drop lands on the substrate is 0 and the surface tension energy is constant, so the sum of energy is:

$$E_{k0} + E_{p0} = E_{k1} + E_D \tag{6}$$

where E_{k1} is the kinetic energy of the droplet just before the impact on the substrate and E_D is the drag energy. The drag force determines the drop deformation and the diameter change, therefore at a high deformation value the drop breakup phenomenon is generated and the drops turn into satellite-type drops. The drag coefficient (C_D) is necessary in order to calculate drag energy. The expression to find this coefficient is shown in Eq. (7).

$$C_D = \frac{24}{Re}(1 + 0.27Re)^{0.43} + 0.47\left[1 - \exp\left(-0.04Re^{0.38}\right)\right] \tag{7}$$

The energy drag is given by Eq. (8). Where ρ_a is the density of the media (air to this case), V is the instantaneous speed and dz is the differential of distance between the print head and the substrate.

$$E_D = \frac{1}{2}C_D\rho_f \frac{\pi}{4}D_0^2 V^2 dz \tag{8}$$

To calculate the energy consumed by the drag effect, the velocity in each moment of travel is required. This is given that the drag coefficient is the function of the Reynolds number, and the Reynolds number is the function of the velocity. Finding the instantaneous velocity is a necessary iterative method. Equation (9) is applied to find the instantaneous velocity.

$$m\frac{\Delta V_z}{\Delta t} - B + C\left(\frac{\Delta V_z}{\Delta t}\right)^2 = 0 \tag{9}$$

where $B = mg$ and $C = \frac{1}{2}C_d\rho_a\left(\pi\frac{D_o^2}{4}\right)\left(\frac{1}{2}\right)^2$

This equation gives the result of the vertical displacement with the respective velocity and time of flight; also, the horizontal displacement calculation should be included and will be discussed later.

The effect of drop breakup, is a phenomenon that is present in drops of different volume, but is caused by other fluid properties such as surface tension, density, and viscosity, is also affected by the initial speed at which the drop is expelled. As mentioned at the beginning of the chapter, these properties are related to the number of Reynolds, Weber and Ohnersorge. The number We and Oh are used to conclude the behavior of the drop while making the trip from the head to the substrate. In [33] five different types of drop breakup are presented and are shown in Fig. 2. In [34] the different types of drop breakup are relationed with the Weber number as shown in the Table 1. Then to get a printable fluid, the components are balanced so that not only does it fulfill the function, but it should have a Weber number below 15.

When the bubble has been jetting at large distances from the free surface the droplet may experience a secondary breakup, which is not desirable with regard to the inkjet printers where satellite-free droplet formation is of high importance from the viewpoint of printing efficiency [35].

When the droplet hits the substrate, a spreading of the fluid occurs on the surface. This spreading can be expressed with a factor β_{max}, that depends on several factors such as: physical characteristics of the fluid, initial energy and the energy of the substrate [36, 37, 38].

The deformation ratio of the droplet is given by Eq. (10).

$$D_{max} = D_o * \beta_{max} \tag{10}$$

The energy of the surface tension can be expressed as Eq. (11).

$$E_s = \sigma\left(\frac{\pi}{4}\beta_{max}D_o\left(1 - cos(\theta_{eqm})\right) + \frac{2D_o^3}{\beta_{max}}\right) \tag{11}$$

At the moment of impact and maximum deformation E_{K2} kinetic energy can be considered zero. Considering a model in which the droplet will be a truncated sphere after the impact with a constant volume [39], is as follows:

$$\beta_{max} = \sqrt{\frac{We + 12 + 3(f_s - \cos\theta)\left[\frac{4\sin^3\theta}{2-3\cos\theta+\cos^3\theta}\right]^{2/3}}{3(f_s - \cos\theta) + 4^{We}\frac{1}{\sqrt{Re}}}} \tag{12}$$

where $f_s = \frac{2(1-\cos\theta)}{\sin^2\theta}$.

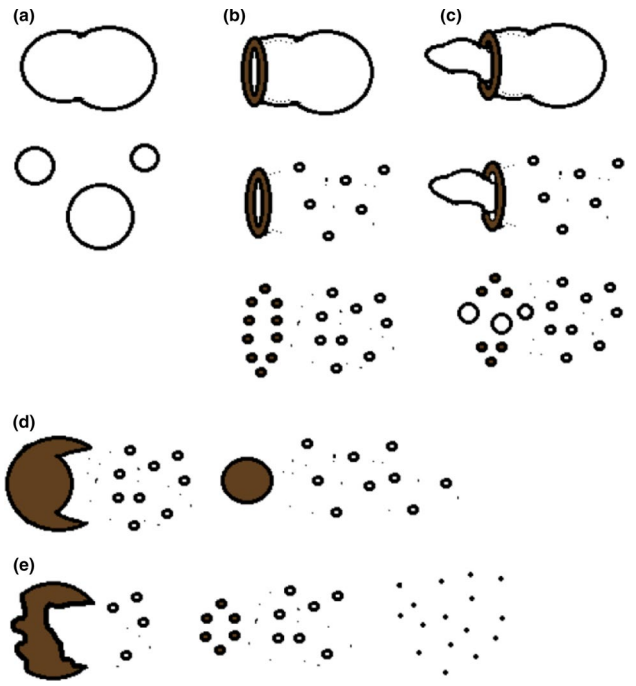

Fig. 2 Newtonian drop breakup morphology. **a** The vibrational behavior of the droplets of a fluid exerts this behavior when it is in the Weber interval between 0 < We < 11. **b** The bag-like behavior of the droplets of a fluid exerts this behavior when it is in the Weber interval between 11 < We < 35. **c** The multimode behavior of the droplets of a fluid exerts this behavior when it is in the Weber interval between 35 < We < 80. **d** The Sheet-thinning behavior of the droplets of a fluid exerts this behavior when it is in the Weber interval between 80 < We < 350. **e** The Catastrophic behavior of the drops of a fluid exerts this behavior when Weber is superior to 350

Table 1 Transition We for Newtonian drops with Oh < 1

Vibrational	0 < We < ~ 11
Bag	~ 11 < We < ~ 35
Multimode	~ 35 < We < ~ 80
Sheet-thinning	~ 80 < We < ~ 350
Catastrophic	We > ~ 350

2.2 CAD method

The distance of the print head to any desired point of the substrate is an important parameter in order to find the energy losses of the droplet, and the correction of the print error as well. There are several methods in which this distance can be found. For the test, a truncated cylinder and a triangular prism were selected. These solids present less correlated information and shown in Fig. 1. Some of these are: (a) Geometric relationships between the print and the solid (substrate). (b) The profile of the surface in the plane X–Y, whichhas analytic equations of lines representing the profile. (c) A CAD model of the substrate. The method used inthis investigation is the CAD method.

The CAD method consists of a file with the threedimensional model of the substrate. It is an interactive process since each one that wants to perform a new job, must access several computer applications. For this, a model is obtained by CAD software, and is used when the substrate is going to be manufactured or by 3D scans when the substrate has been manufactured and there is no previous CAD file or technical drawings. Once the CAD file is obtained, it is necessary to process the surface of the substrate, and export it into a generic file. For this investigation, STL files are used. STL is a generic file developed for stereo lithography and has recently been used in 3D printing.

The STL format describes the surface of a solid as if it were composed by triangles. Each information pack starts with the text "facet normal", and then there are three numerical values corresponding to the orientation of the normal vector to the surface of one triangle. Next, the text "outer loop", the information of the three vertexes and the text "end loop". Next, the text "end loop". The package is closed by the text "end facet".

In [40], it is shown that the STL format is a set of facet descriptions in the ASCII format that contains its normal unit vector and 3D coordinates of three vertices. The content of an STL file text is readable, and its file size is so large that it is generally used as a test tool. The structure of the STL format is as follows:

solid solid_name
<facet list>
facet normal [$N_x N_y N_z$]
  outerloop
    vertex[$X_1 Y_1 Z_1$]
      vertex[$X_2 Y_2 Z_2$]
    vertex[$X_3 Y_3 Z_3$]
  endloop
endfacet
endsolid

The algorithm in Fig. 3 presents the procedure to obtain the "Zt" distance between the print head and the curved substrate. The algorithm uses the points of the vertices found in the STL file of substrate in which the printing was made, takes the data as a string and performs the match pattern action to be able to extract the alphabetic characters and only use the numeric characters. After obtaining the numeric characters, it is necessary to make comparisons between points "Xini" and "Yini" and store the points closest to these

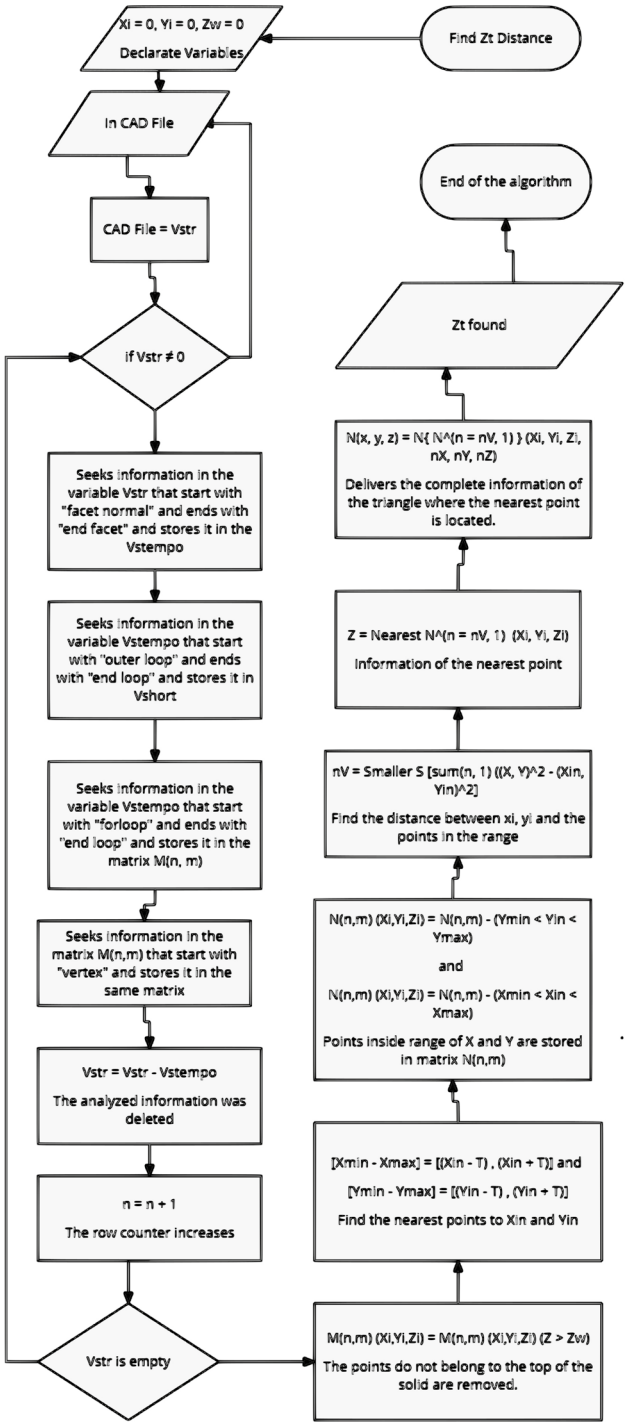

Fig. 3 Algorithm with the function of finding the distance from the highest point of the solid in which the printing will be made, to the nozzles of the head. This distance is defined as "Zt"

in a matrix, and finally use these points to find points "X", "Y" and "Z" that correspond to the vertex in which the

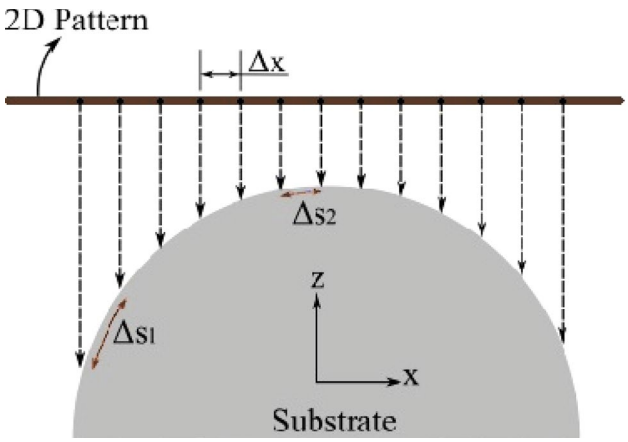

Fig. 4 The ratio in distance of two nearby points in a 2D plane changes once they are adjusted for the 3D substrate

distance of "Zt" is located, which is the distance between the substrate and the print head.

2.2.1 Error correction of 2D pattern to 3D

As a consequence of a pattern printing onto non-flat substrates, two errors are presented: the error given the conversion of 2D pattern to 3D, and the error due to the parabolic movement of the droplet. The mathematical models of the two errors is presented.

Given a 2D print pattern, the projection of the print pattern onto the curved substrate tends to deform the original pattern due to the distance between points. As Fig. 4 exposes, the projection of the 2D pattern on the curved surface tends to present errors in the proportion of the pattern. The released drops on the substrate will produce a distorted pattern at the borders since the drops which were ejected have a greater spacing ($\Delta s > \Delta x$). As the print head advances to where the curvature is less pronounced, the distortion is less because the substrate is almost flat ($\Delta s \approx \Delta x$). Figure 4 is a general tool for evaluating any substrate and analyzing the possible implications in the compensation process to analyze the ratio of distance between two close points of 2D to a 3D surface according to the angle of the 3D surface. To achieve good quality printing (including the pattern proportions), it is necessary to adjust the 2D pattern to constantly keep the pattern onto the 3D surface. As Fig. 4 shows, the distance of Δx_0 has to be modified to keep Δs_0 constant. The compensation has to be in x as the direction of the printhead and y is the substrate depth. The surface of the substrate is divided by straight lines. As a consequence, the surface of the substrate is represented as a sequence of straight lines. As Fig. 5 exposes, the value of $\sqrt{\ }\Delta s$ is calculated by the Pythagoras equation ($\Delta s = (\Delta x^2 + \Delta z^2)^{1/2}$). Doing a mathematical

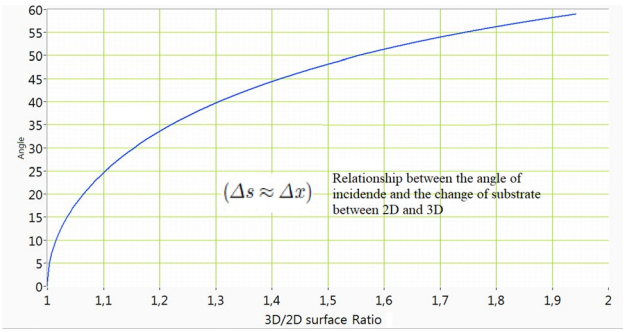

Fig. 5 Comparison of the angle change, when the transition is made between a flat substrate to an on-flat substrate

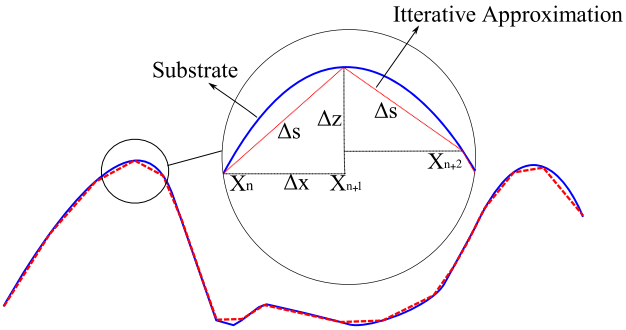

Fig. 6 Iterative approximation to the substrate and Pythagoras mathematical procedure

procedure, it can be found that the next point in x direction (X_n) is given by Eq. (13) and is shown in Fig. 6.

$$X_{n+1} = \frac{\Delta s}{\sqrt{1 + \left[f'(x,y)\right]^2}} + X_n \tag{13}$$

where $f^0(x, y)$ is the derivative of the function of the substrate surface. It also corresponds to the slope in the X-axis direction of the normal vector to the triangle of the STL file, as in the method of the CAD file. This procedure can be applied to the Y-axis direction as well.

The point found X_{n+1} has a large (maximum 12%) error because the slope was obtained with the point of origin. To improve the prediction, the polygon method is added to the above process which uses the midpoint of the initial result and there the derivative is taken which gives a result with a maximum error of less than 0.001%.

The method is iterative and accumulative. Any new point depends on the previous case, which has just been modified. Assuming m is one of the py lines, parallel to the X axis, n a point of the total px of each line, the vector X_m is:

$$[X]_m = V_{n=1}^{n=px}\left(X_{n+1} = \frac{\Delta s}{\sqrt{1 + \left[f'(x,y)\right]^2}} + X_n\right) \tag{14}$$

The complete matrix is exposed in Eq. (15).

$$[M]_x = M_{m=1}^{m=py}[X]_m \tag{15}$$

The compensation matrix in both directions is given by

$$M_{x,y}^{px,py} = \left[X_{(n,m)}, Y_{(n,m)}\right].$$

The second compensation is performed on the travelling droplet, influenced by the speed and movement of the print head. In scanning machines, the print head movement is in the direction of the one axis. Most printers have the option of printing in both directions of the machine. On a single pass machine, the substrate moves, at a constant horizontal relative velocity between the drops and substrate. As a consequence, there is no parabolic trajectory, but there is a distortion due to the difference in the vertical trip between drops. The movement of the drop leaving the head is parabolic as shown in Fig. 1. The compensation method predicts the point where the print head should launch the drop; as a consequence, an independent travel is placed at the corresponding point. This procedure is added to $P_{(x,y)}$ points of the first compensation and execute the algorithm presented in the Fig. 4. The initial velocity of the drop V_x is equal to the print head velocity. Also, the drop velocity is affected by the collision with the air molecules of oxygen and nitrogen, therefore, the droplet velocity in X direction is given by Eq. (16).

$$\Delta X^{00} = {}^{X}\left(V_x + \Delta V_x\right)\Delta t \tag{16}$$

The different parts of the substrate should be observed the possible measures that can be considered to achieve an adjustment between the substrate and the print head. These measurements are shown in Fig. 7. After taking these measurements for the location of the head into account, it must be achieved that the final conditions of the horizontal travel are limited by the variable Z, until the drop reaches the substrate or Z = Zt.

$$P_{x,y}^{00} = P_{x,y}^{0} - \Delta X^{00} \tag{17}$$

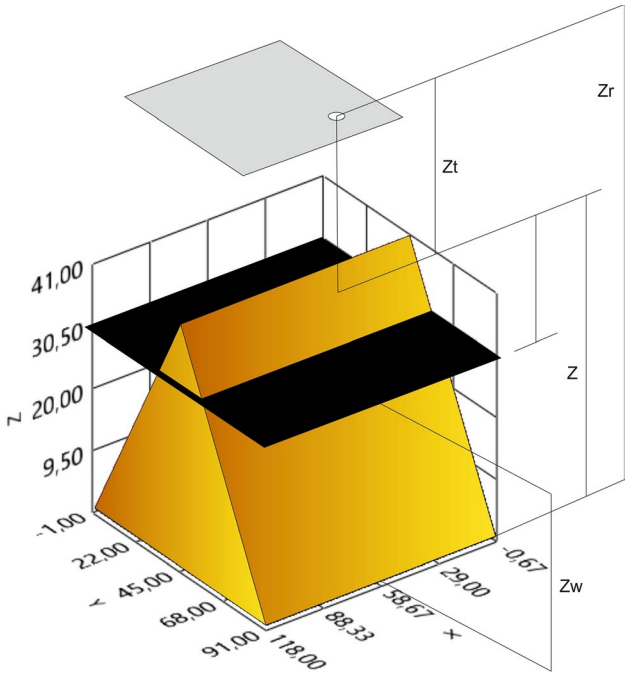

Fig. 7 Different measurements taken into account to carry out the printing process and how the solid cutting is done, which is being reconstructed in the engineering software

3 Results and discussion

In this section different theoretical and practical tests are shown. These tests were performed with a Xaar® 1001 printhead; as a substrate, a triangular prism and a truncated cylinder were used, in which parameters must be taken into account to define the relative quality of printing, which in this case is argued by non-flat substrates.

3.1 Theoretical tests

In Sect. 3, the impact of kinetic energy is analyzed on the final speed of the drop. This energy is influenced by the volume of the drop. In Fig. 8, the relationship between volume and speed is evidenced. e.g. after 4 ms, the speed loss for a drop with a volume of 150 pL is 32%, while a drop of 6 pL has a loss of 94% and after 12 ms, the gravity is the only factor influencing its velocity until it impacts the substrate. Due to the long movement an expected result was the influence of the gravity in the change of speed of the drop. The difference in the data, taking into account the gravity or eliminating it, is no higher than 1–2%.

The distance covered in two axes is influenced by the volume of the drop as well; Fig. 9 shows the distance traveled by different sizes of drops with the same initial speed and horizontal print head carriage speed. If the vertical distance is 20 mm, the travel proportion of two drops in the X direction is 3/1 when the volume is 150 and 15 pL. Drops of 6 pL stop the horizontal flight at 12.3 mm of the vertical movement. The results indicate there is a direct relation between the volume of the drop and the maximum vertical movement to avoid drops stopping the horizontal flight before the travel has finished. (For each initial speeds in Z and X of drops).

The altitude of city where the printing is done also influences the horizontal flight of the drops. In Fig. 10 the theoretical results of seven prints made in environments from 0.745 to 1.0 atmosphere is presented. E.g. for a vertical travel of 20 mm and with a speed print head carriage of 15 m/min the horizontal flight is duplicated between values of 0.745 and 1.0 atm.

Now the influence of the ink density in the results of the horizontal flight of drops is shown. Figure 11 shows

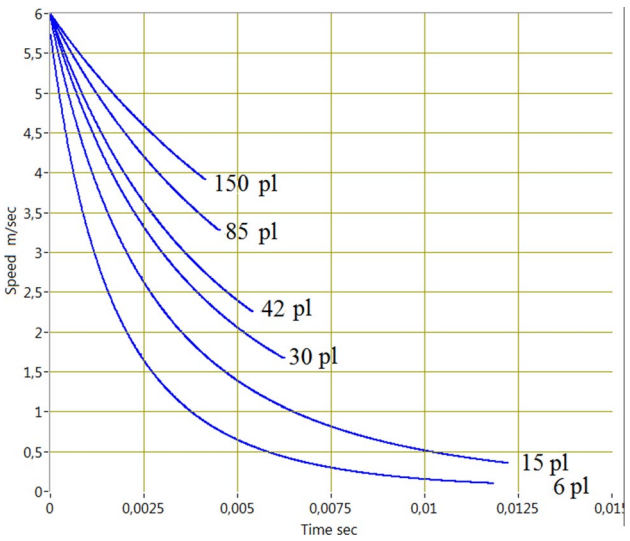

Fig. 8 The relationship between volume and speed

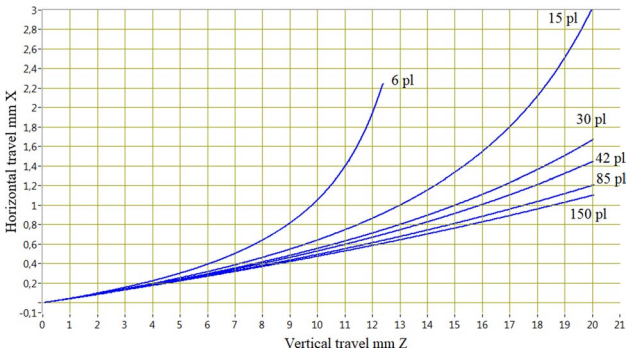

Fig. 9 Horizontal flight X and vertical journey or movement Z of drops with 6 m/s initial speed and initial horizontal print head speed of 15 m/min

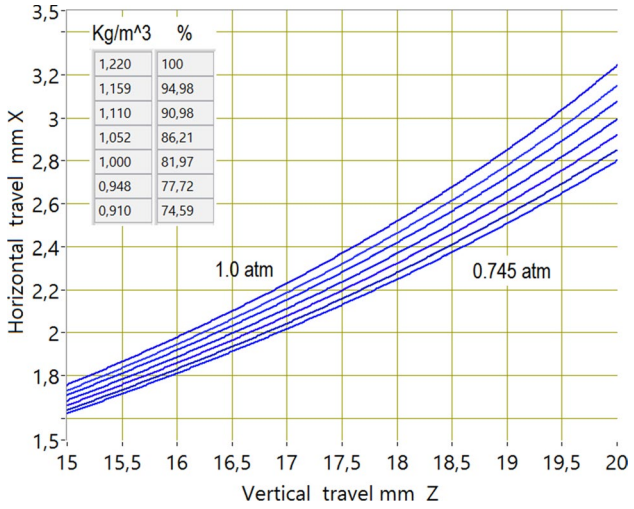

Fig. 10 Influence of the altitude in the horizontal travel of a drop due to the air density. Parameters 15 pL, 1, 2 ink density, 15 m/min substrate speed, 20 mm vertical travel

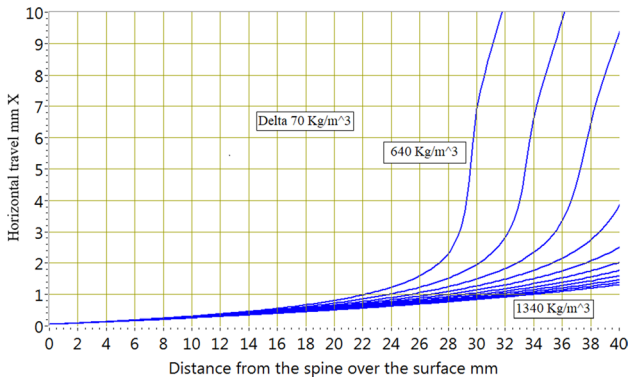

Fig. 11 Influence of ink density in the horizontal travel of a drop

the theoretical result of nine prints with densities from 640 to 1340 kg/m^3 and parameters: 42 pL, 6 m/s initial drop speed, 9 m/min substrate speed, 25 mm vertical movement, 0.84 atmosphere and a temperature of 24–26 centigrades, type case c) Fig. 1. Inks with low density rapidly lost their vertical speed and became similar to a shower of disorderly drops which is difficult to predict where they will fall. If the initial drop speed is reduced, the shower effect moves to the left reducing the reach of the drops.

3.2 Validation experiments

Experiments were conducted with print head type Xaar® 1001 GS12 over truncated cylindrical and wedge substrates covered with graph paper as it is observed in Fig. 12. This printer has a mobile bed in which the substrate is fastened and the print head carriage moves in the other Cartesian direction to change the swath to print. Due to this

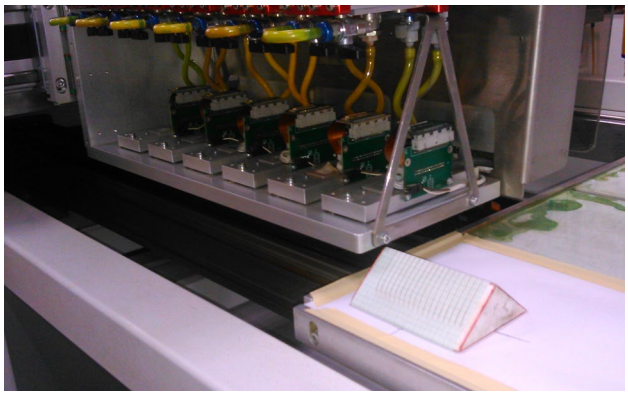

Fig. 12 Test prints on a truncated wedge substrate base 118 × 91 mm, height 41 mm

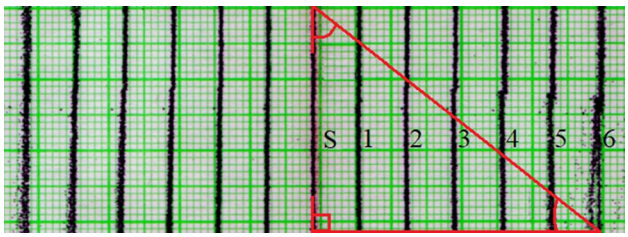

Fig. 13 Reduction of quality, in front of the change of height of the print head to the substrate and the data is shown in Table 2

characteristic, the horizontal flight of the drops and its associated friction with air do not exist. Vertical travel and its associated friction with air should be considered.

To define the best quality print and from it determine the quality changes, is used the result when the print head is nearest the substrate. This event is given when the long side of the print-head is over or co-lineal with spine of the substrate, and is shown in the Fig. 13.

The relative quality is reflected in all the experiments, where as defined above, the impression of the spine is considered, with 100% quality, and it decreases as the spindle is farther from the substrate, this decrease in quality is conditioned directly with the drop breakup phenomenon.

Parameters for non-flat surfaces were taken into account to define the best relative quality. The distance between the head and the spine of the solids must be less than 2 mm, with this distance the best quality is obtained on the solid, which means that it complies with 100% of the defined relative quality. As the head moves away from the back of the solid the height grows linearly (triangular prism) and non-linear for the other solid (truncated cylinder).

The direction of printing is taken account because it allows to evaluate different influences in the final impression, for example, when printing in the direction of the spine of the solid, it is essential the speed of the head relative to

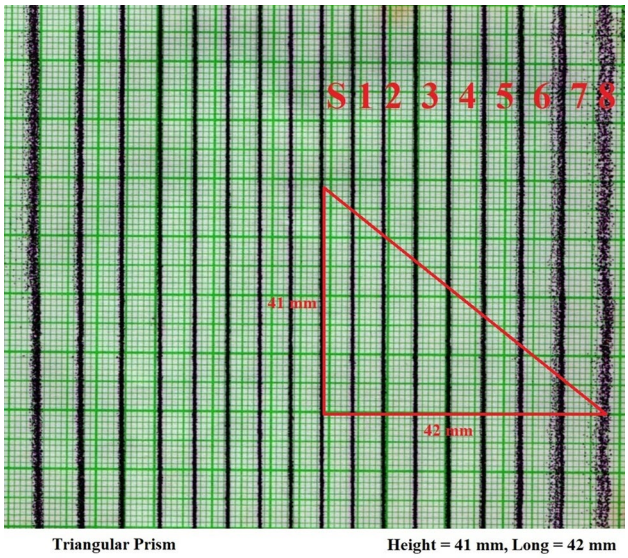

Fig. 14 Unfolded substrate of printed figure constituted by parallel lines in a print case a) of Fig. 1

the substrate, but when prints in a direction perpendicular to the spine of the solid the phenomena of distance between the head and the substrate are those that prevail.

In Fig. 14, a practical test of a print of a group of parallel lines separated by 5 mm is presented. The case of impression corresponds to case a) in Fig. 2. The speed of the print head carriage is slow (1 m/min) to minimize the influence of the drop flight and to maximize the influence of 2D–3D presented in the Fig. 5. Now the distance between lines multiplied by 1.32 gives 6.6 which correspond to the distance between the parallel lines and validates the 2D to 3D compensation. It is also observed that the quality is decreasing when the printhead moves away from the substrate, when "S" is the top of the susbtrate and "8" is the bottom (Table 2).

In Fig. 15, the result of the same test but with a truncate cylinder as the substrate is presented in, case b) in Fig. 1. In this case, the slope is variable as it is presented in Table 3.

Table 2 Data to define the relative quality of printing

Printed line	Height (mm)	Relative quality (%)
S	2	100
1	5	80
2	12	60
3	18	40
4	24	20
5	31	10
6	38	0

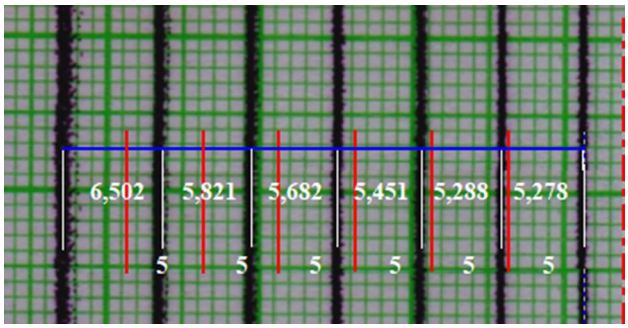

Fig. 15 Unfolded substrate of printed figure constituted by parallel lines in a print case b) of Fig. 1

The swaths formed by the lines from the center of the spine have an average slope in degrees, and each slope has a corresponding ratio that is multiplied by the distance between lines giving the distance in the substrate.

Four tests were conducted with the result presented in Fig. 15 and graph of Fig. 16. The theoretical (black) and the practical tests do not overlap, but they show the same pattern and indicate that there are some details missing which must be researched.

The main test was conducted maximizing the effect of the speed of the print head carriage and the distance from print head to substrate. In this case, the initial drop speed was 5.5 m/s, the print head carriage speed was 1, 5, 10, 15, 20 and 24 m/min, 84 pL train drops and brown reference TEB-16617 Colorobbia R ink with 1358 kg/l density and 14.5 cP viscosity. The impression was over a truncated wedge in the same direction of the spine as in case c) of Fig. 1. The results show that the distance between lines tends to keep a constant, but the shape of the line changes to a curve. In Fig. 17, from the spine, moving right, the distance print head-substrate is higher and the drops fall later on. The direction of the substrate movement is from top to bottom of Fig. 17.

It is also observed that from 30–40 mm of the spine, which correspond to heights Zt of 27–36 mm, the drops start to separate from the main line forming satellite drops. Even so, it is possible to graph the practical result and to compare with various theoretical curves.

For each point of a curve, 8 measurements were taken. After the average was registered and using fitting function, the equation of the test was constructed. Experimental four order polynomial equations are listed in Table 4. The experimental results are presented in the graph Fig. 18. The curves in this graph present an inflection at the end that is not presented in the theoretical tests. The reason is that the mathematical model does not include the atomization phenomenon which changes the dynamics of the results.

Figure 19 shows a test with slow print head carriage speed (1 m/min). In this, the line preserves its linearity until

Table 3 Theoretical variables to be compared with practical results

Position	1	2	3	4	5	6	7
Distance	2.5	7.5	12.5	17.5	22.5	27.5	32.5
Zt	2.06	2.56	3.58	5.16	7.34	10.2	14.0
Angle	2.86	8.62	14.4	20.05	26.7	33.4	40.5
Ratio	1.001	1.01	1.03	1.07	1.12	1.19	1.31
3D distance	50	50	52	53	56	60	66

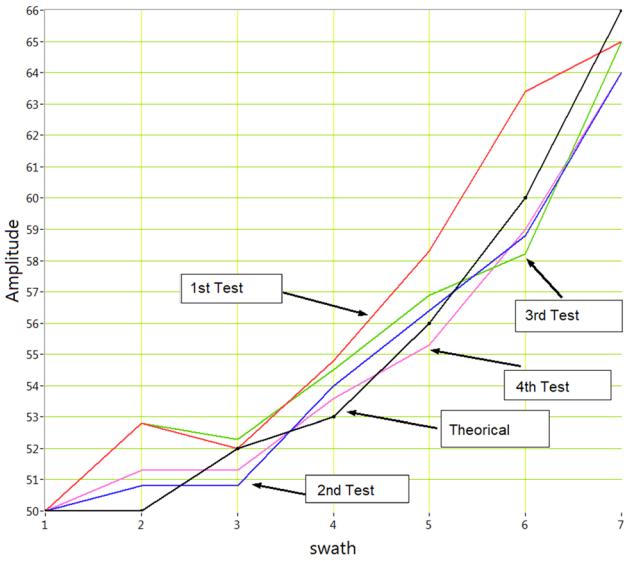

Fig. 16 Graph with the comparison between the theoretical (black) and practical results

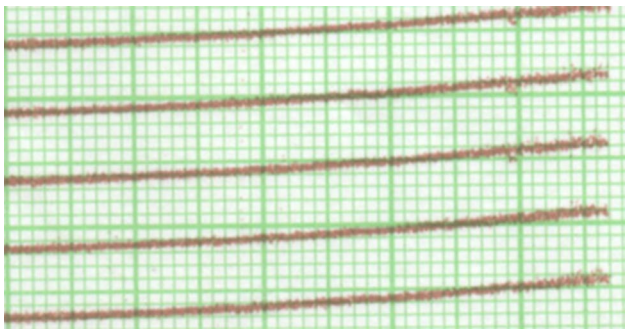

Fig. 17 Printing on wedge substrate, 15 m/min print head carriage speed, with print head movement co-linear to the spine (case c Fig. 1)

30 mm from the spine of the substrate which is good news, but the productivity would be low. The lines also gain thickness due to the lack of accuracy of the drop with time of flight.

In Fig. 20, the result of a print using three ink color is presented. The density of each ink is: black 1.3 kg/l, red 1.27 kg/l and brown 1.35 kg/l, print head carriage 9 m/min, 84 pL train drops, 0.84 atmosphere, 40°–42° in temperature, case c Fig. 1. The lines of different color are overlapping in

Table 4 Coefficients of experimental curves

Speed	X0	X1	X2	X3	X4
Curve (m/min)					
24	6.95E−3	1.65E−2	4.56E−3	1.70E−4	2.21E−6
20	−1.79E−2	5.01E−2	−8.57E−4	2.98E−5	−2.91E−8
15	1.98E−3	6.90E−3	2.56E−3	−7.5E−5	9.91E−7
10	0	1.45E−2	1.1E−3	−4E−5	7E−7
5	−3.85E−3	4.04E−2	−1.81E−3	5.40E−5	−4.54E−7
1	1.31E−3	5.58E−3	7.83E−4	−3.69E−5	4.95E−7

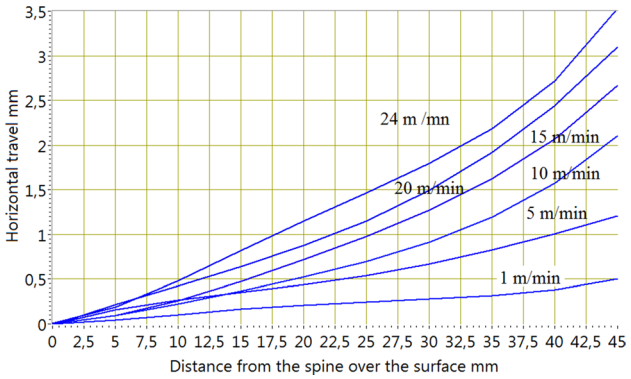

Fig. 18 Experimental results using different print head carriage speeds

the original figure. The lines in the substrate do not appear to be overlapping. The reason is the difference in the physical properties of the inks; those differences being the density and mainly surface tension. For density, heavier drops in a sphere of less frontal area lose less dynamic energy in the movement, and resulting therefrom, the flight in a horizontal direction is shorter. For superficial tension, the Weber number gives indications of the length of the movement before the drop breakup.

In Fig. 20, after 15 mm from the spine of the truncated solid (equivalent to a vertical drop of 15.08 mm), the black drops breakup and become smaller, and as a consequence, suffer stronger deceleration because of falling in different places. The effect of the superficial tension is not equal for the inks; the black ink (Endeka® 1,3k/l), despite having higher density than red ink, has a shorter trip before

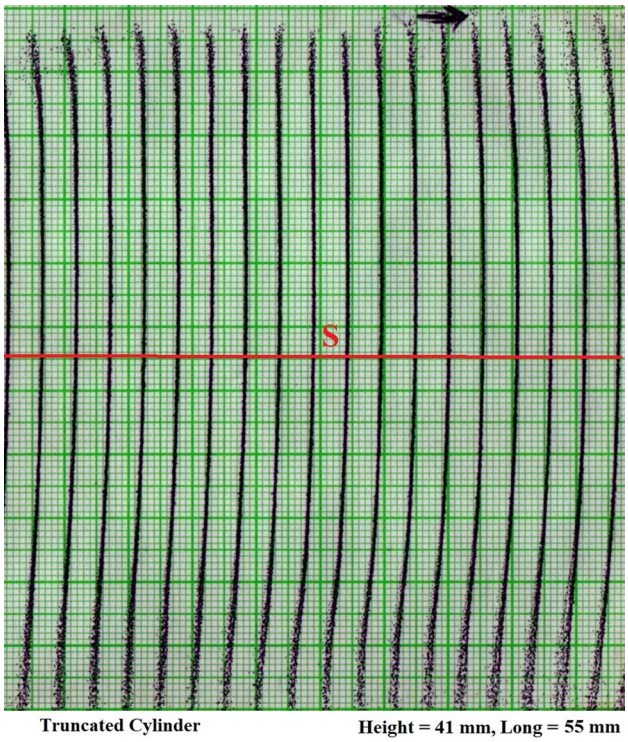

Fig. 19 Printed lines in a truncated cylinder, print head displacement parallel to the spine of substrate, case d) of Fig. 1, print head carriage speed of 1 m/min

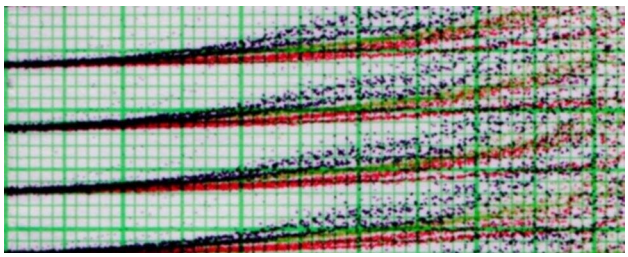

Fig. 20 Printing with different ink colors in the same pattern showing no overlapping (case c Fig. 1)

breakup. The tension of the inks tested is around 10–20 cP and the print head of the printer can works 7–30 cP, which gives range to increase the superficial tension and preserving the Ohnesorge number in range and to achieve a higher ink movement without atomization.

Print head tested are constituted by two rows of nozzles separated by some micron and most of the print head have two or more rows. The control does an electronic count of the print head carriage displacement to guarantee two drops in different rows fall on the same line. When vertical distance is high and there is air turbulence or low print head carriage speed, both rows of drops fall in a different position forming capricious curves as showed in Fig. 21.

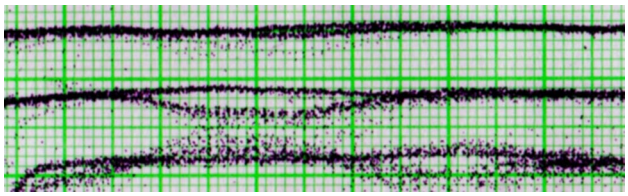

Fig. 21 Printing defects due to air turbulence. Drop initial speed 5.5 m/s, print head carriage 1 m/min. Case Fig. 1

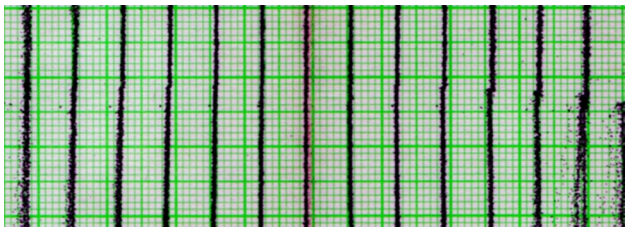

Fig. 22 Printing defects due to the mechanical lack of repeatability. Drop initial speed 5.5 m/s, print head carriage 9 m/min. Case a) Fig. 1

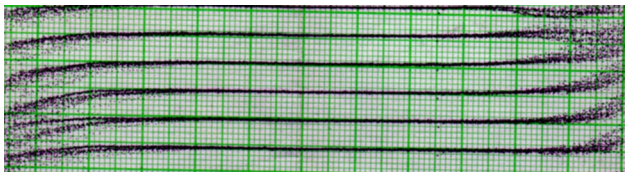

Fig. 23 Printing defects orientation due to the print direction. Drop initial speed 5.5 m/s, print head carriage 1 m/min. Case c) Fig. 1

Due to the fact that the print head is more distant to the substrate, the precision of the mechanical part of the printer will be greater because the distance becomes a multiplier of mechanical errors. In Fig. 22, discontinuities are observed in the lines due to an induced difference in the location of the print head carriage in two swaths and shows an example of the relative quality used in this test.

Figure 23 shows how a print without compensation, two swaths with different print direction suffer a distortion in different orientation. Another situation presenting a close result is when the print head carriage speed is too low.

4 Conclusions

- In this investigation the results were obtained using an interactive method of multiple man-machine relations, which has a common structure, many engineering problems begin with mathematical models and end with the

change of a physical equipment that is controlled by computer.

- In this article, the final position of a drop expelled by a print head to a non-planar substrate was analyzed taking into account the physical, kinematic and dynamic properties affecting the trip of the drop. The range in which the results work is outside of the regular quality in the field of printing. As this is the first approach, it can not get inside the range of the standard quality; and for that reason it was used a relative quality that has as objective to evaluate the improvement with the proposed methods. The result can be used for low resolutions products
- The printed image of a print-file over a non-flat substrate has as result a deformed image. To process the information so could be developed a method of correction, it was necessary to extract each print point information from the Raster Image Processor (RIP). Using mathematical models the points are relocated and printed as a distorted image that over non-flat substrate is seen correct. Each point coordinates is processed according to the height, the relative velocity between the substrate and print head, and the properties of the fluid. After each point is processed a new coordinates become the compensates and the original figure now is seen distorted if it is printed distorted in the display or if it is printed in a flat surface.
- The droplet velocity is diminished by the drag force. Droplets with less volume relative to the front area lose speed more quickly. Drops of a gray-scale system form a train, then have more volume relative to the area exposed to the drag force.
- The drops in trips with two components of initial velocity, the velocity of exit of the print-head and the relative speed print-head-substrate, generate changes of location in the substrate having like main variable the volume of the drop, the relative speed printhead-substrate and the vertical travel distance.
- The atmospheric pressure modifies the density and proportionally the drag force. Then, at higher altitudes, the speed loss is less. A height of 3000 meters above sea level only decreases about 10% of the pressure, then the change is not very representative.
- The experiments validate the mathematical formulation in relation to the change of the drop point as a function of the parameters and the height as the main variable. The drops according to the height have suffered once or several times from the drop breakup phenomenon.
- The density of the fluid influences the loss of velocity of the drop. With a head drop drop speed, the higher density the drop has higher initial energy. Inks with low densities lose 100% of their energy before reaching the substrate.
- The displacement of the head that moves the printheads produces air generating a pushing force that becomes an inconvenience for long distance trips where the drop has lost a high percentage of its kinetic energy.
- The drop breakup model was incorporated but was not positively validated because the drops traveled much longer trajectories than those predicted by different models of the phenomenon described in the literature. The possible cause and reason for future work may be the cylindrical shape due to the grayscale and the solid particles inside the fluid that act as pellets.
- The use of functional fluids is very limited, because the physico-chemical conditions force the number of Weber to be within a small range, to prevent the occurrence of the Drop Breakup phenomenon, making the trip to occur several anticipating that during the trip the vibrational phenomenon will occur several times throughout. To the future is need investigate the effect of the cylindrical drops, formed by grayscale in the theory establish for this field. Also the effect of big pieces of pigment that make part of the modern the functional fluids.

References

1. Wang, C.-T., Huang, K.-Y., Lin, D.T., Liao, W.-C., Lin, H.W., Hu, Y.-C.: A flexible proximity sensor fully fabricated by inkjet printing. Sensors **10**(5), 5054–5062 (2010)
2. Komuro, N., Takaki, S., Suzuki, K., Citterio, D.: Inkjet printed (bio) chemical sensing devices. Anal. Bioanal. Chem. **405**(17), 5785–5805 (2013)
3. Lorber, B., Hsiao, W.-K., Hutchings, I.M., Marti, K.R.: Adult rat retinal ganglion cells and glia can be printed by piezoelectric inkjet printing. Biofabrication **6**(1), 015001 (2013)
4. Xu, T., Jin, J., Gregory, C., Hickman, J.J., Boland, T.: Inkjet printing of viable mammalian cells. Biomaterials **26**(1), 93–99 (2005)
5. Shirazi, S.F.S., Gharehkhani, S., Mehrali, M., Yarmand, H., Metselaa, H.S.C., Kadri, N.A., Osman, N.A.A.: A review on powder-based additive manufacturing for tissue engineering: selective laser sintering and inkjet 3d printing. Sci. Technol. Adv. Mater. **16**(3), 033502 (2015)
6. Ozkol, E.: Rheological characterization of aqueous 3y-tzp inks optimized for direct thermal ink-jet printing of ceramic components. J. Am. Ceram. Soc. **96**(4), 1124–1130 (2013)
7. Arango, I., Betancur, M., Bonil, L., Acevedo, D.: Impresion digital inkjet sobre formas cilındricas con tintas uv. *Manufactura flexible*, p. 109
8. Rahul, S.H., Balasubramanian, K., Venkatesh, S.: Optimizing inkjet printing process to fabricate thick ceramic coatings. Ceram. Int. **43**, 4513 (2016)
9. Arazn, A., Janeczek, K., Futera, K.: Mechanical and thermal reliability of conductive circuits inkjet printed on flexible substrates. Circuit World **43**(1), 9 (2017)
10. Ikegaw, M., Ishii, E., Harada, N., Takagishi, T.: Development of ink-particle flight simulation for continuous inkjet printers. J. Manuf. Sci. Eng. **136**(5), 051021 (2014)
11. Yeo, L.P., Lok, B.K., Nguyen, Q.M.P., Lu, C.W., Lam, Y.C.: Selective surface modification of pet substrate for inkjet printing. Int. J. Adv. Manuf. Technol. **71**(912), 1749–1755 (2014)

12. Fathi, S., Dickens, P.: Droplet analysis in an inkjet-integrated manufacturing process for nylon 6. Int. J. Adv. Manuf. Technol. **69**(1–4), 269–275 (2013)
13. Ozkan, M., Dimic-Misic, K., Karakoc, A., Hashmi, S.G., Lund, P., Maloney, T., Paltakari, J.: Rheological characterization of liquid electrolytes for dropon-demand inkjet printing. Organic Electron. **38**, 307–315 (2016)
14. Wijshoff, H.: Structure-and Fluid-Dynamics in Piezo Inkjet Printheads. University of Twente, Enschede (2008)
15. Vaezi, M., Seitz, H., Yan, S.: A review on 3d microadditive manufacturing technologies. Int. J. Adv. Manuf. Technol. **67**(5–8), 1721–1754 (2013)
16. Huang, S.H., Liu, P., Mokasdar, A., Hou, L.: Additive manufacturing and its societal impact: a literature review. Int. J. Adv. Manuf. Technol. **67**(5–8), 1191–1203 (2013)
17. Campbell, P.G., Weiss, L.E.: Tissue engineering with the aid of inkjet printers. Expert Opin. Biol. Therapy **7**(8), 1123–1127 (2007)
18. Subbaraman, H., Pham, D.T., Xu, X., Chen, M.Y., Hosseini, A., Lu, X., Chen, R.T.: Inkjet-printed twodimensional phased-array antenna on a flexible substrate. IEEE Antennas Wirel. Propag. Lett. **12**, 170–173 (2013)
19. Perelaer, J., Hendriks, C.E., de Laat, A.W.M., Schubert, U.S.: One-step inkjet printing of conductive silver tracks on polymer substrates. Nanotechnology **20**(16), 165303 (2009)
20. Y-a, J., He, Y., Gao, Q., J-z, F., G-q, F.: Droplet deviation modeling and compensation scheme of inkjet printing. Int. J. Adv. Manuf. Technol. **75**(9–12), 1405–1415 (2014)
21. Friederich, A., Binder, J.R., Bauer, W.: Rheological control of the coffee stain effect for inkjet printing of ceramics. J. Am. Ceram. Soc. **96**(7), 2093–2099 (2013)
22. Arango, I., Canas, M.: Dynamic analysis of a recirculation system of micro functional fluids for ink-jet applications. Microsyst. Technol. **23**(5), 1485–1494 (2017)
23. Krieger, I.M., Dougherty, T.J.: A mechanism for non-newtonian flow in suspensions of rigid spheres. Trans. Soc. Rheol. **3**(1), 137–152 (1959)
24. Poletto, M., Joseph, D.D.: Effective density and viscosity of a suspension. J. Rheol. **39**(2), 323–343 (1995)
25. Rodriguez-Rivero, C., Castrejon-Pita, J.R., Hutchings, I.M.: Aerodynamic effects in industrial inkjet printing. J. Imaging Sci. Technol. **59**(4), 40401–1 (2015)
26. Barnett, D., McDonald, M.: Evaluation and reduction of elevated height printing defects. In: NIP and Digital Fabrication Conference, vol. 2014, pp. 38–43. Society for Imaging Science and Technology (2014)
27. Hsiao, W.K., Martin, G.D., Hoath, S.D., Hutchings, I.M., Hook, M., Massucci, M.: Evidence of print gap airflow affecting web printing quality. In: Society for Imaging Science and Technology, NIP and Digital Fabrication Conference, vol. 2013, pp. 303–306 (2013)
28. Link, N., Lampert, S., Gurka, R., Liberzon, A., Hetsroni, G., Semiat, R.: Ink drop motion in wide-format printers: ii. airflow investigation. Chem. Eng. Process. Process Intensif. **48**(1), 84–91 (2009)
29. Pilch, M., Erdman, C.A.: Use of breakup time data and velocity history data to predict the maximum size of stable fragments for acceleration-induced breakup of a liquid drop. Int. J. Multiph. Flow **13**(6), 741–757 (1987)
30. Theofanous, T.G., Mitkin, V.V., Ng, C.L.: The physics of aerobreakup. iii. Viscoelastic liquids. Phys. Fluids **25**(3), 032101 (2013)
31. Barone, S., Casinelli, M., Frascaria, M., Paoli, A., Razionale, A.V.: Interactive design of dental implant placements through cad-cam technologies: from 3d imaging to additive manufacturing. International Journal on Interactive Design and Manufacturing (IJIDeM) **10**(2), 105–117 (2016)
32. Wu, H.-C., Shan, T.-R., Hwang, W.-S., Lin, H.-J.: Study of microdroplet behavior for a piezoelectric inkjet printing device using a single pulse voltage pattern. Mater. Trans. **45**(5), 1794–1801 (2004)
33. Guildenbecher, D.R., Lopez-Rivera, C., Sojka, P.E.: Secondary atomization. Exp. Fluids **46**(3), 371 (2009)
34. Hsiang, L.-P., Faeth, G.M.: Near-limit drop deformation and secondary breakup. Int. J. Multiph. Flow **18**(5), 635–652 (1992)
35. Dadvand, A., Shervani Tabar, M.T., Khoo, B.C.: A note on spark bubble drop-on-demand droplet generation: simulation and experiment. Int. J. Adv. Manuf. Technol. **56**(1–4), 245–259 (2011)
36. Roisman, I.V., Rioboo, R., Tropea, C.: Normal impact of a liquid drop on a dry surface: model for spreading and receding. In: Proceedings of the Royal Society of London A: Mathematical, Physical and Engineering Sciences, vol. 458, pp. 1411–1430. The Royal Society, London (2002)
37. Chandra, S., Avedisian, C.T.: On the collision of a droplet with a solid surface. Proc. R. Soc. Lond. A **432**(1884), 13–41 (1991)
38. Hutchings, I.M., Martin, G.D.: Inkjet Technology for Digital Fabrication. Wiley, London (2012)
39. Perelaer, J., Smith, P.J., van den Bosch, E., van Grootel, S.C., Ketelaars, P.H.J.M., Schubert, U.S.: The spreading of inkjet-printed droplets with varying polymer molar mass on a dry solid substrate. Macromol. Chem. Phys. **210**(6), 495–502 (2009)
40. Tong, W., Cheung, E.H.: Enhanced stl. Int. J. Adv. Manuf. Technol. **29**(11–12), 1143–1150 (2006)